Gas generation and intramolecular isotope study in laboratory pyrolysis of the Springfield coal from the Illinois Basin

Xiaoqiang Li[a*], Maria Mastalerz[b], Juske Horita[a]

[a] *Department of Geosciences, Texas Tech University, Lubbock, TX 79409, USA*

[b] *Indiana Geological and Water Survey, Indiana University, Bloomington, IN 47405, USA*

(* Corresponding author: xiaoqiang.li@ttu.edu)

Abstract

Position-specific (PS) isotopes of propane have been proposed as a potential geochemical tool to decipher various geological processes (e.g., thermal cracking, biodegradation, H exchange) in natural reservoirs. The limited studies have been conducted on the PS isotopes of propane from the pyrolysis gases from marine shales, and natural gases sourced from lacustrine and marine kerogens, but little is known on gases produced from the humic kerogen. This study investigated the PS $\delta^{13}C$ of propane in the closed-system pyrolysis of the Springfield coal, Illinois Basin, Indiana, at 310 to 470 °C (Easy $\%R_o$: 0.76 to 3.07). The C kinetic isotope effect (KIE) of CH_4 produced in both this study and previous low-temperature pyrolysis of the same coal indicates the cleavage of C-O bonds is the main generation pathway at the early kerogen cracking stage, followed by the breakdown of alkyl groups. At the wet-gas cracking stage, C_3H_8 production from thermally stable compounds has a significant influence on the bulk and position-specific C KIE in the pyrolysis of marine Woodford kerogen and Springfield coal. According to the PS $\delta^{13}C$ of propane, the central site is likely more enriched in ^{13}C and the $\delta^{13}C$ of the terminal site is relatively

heterogeneous within the propyl group attached to different functional groups of the gas-prone kerogen. Our findings based on the pyrolysis experiments and natural gas samples indicate thermal cracking and biodegradation appear to alter the $\delta^{13}C_{cen}$ values more significantly than the $\delta^{13}C_{ter}$ values of propane. The larger magnitude of $\Delta C_{c\text{-}t}$ in the kMC simulations (Peterson et al., 2018) compared with those from the marine shale and coal possibly implies the non-random distributions of ^{13}C of propane precursors in the kerogens. As a new dimension of intramolecular isotopic information of propane, the PS $\delta^{13}C$ values can contribute to fingerprinting the gas origins and identifying the various geological processes (e.g., kerogen cracking, wet-gas cracking, microbial activities) in sedimentary basins.

Key words: position-specific isotope, pyrolysis experiments, natural gas, gas generation

1 Introduction

Recently, position-specific (PS) isotope of propane has been applied to examine the gas origin and maturity (Suda et al., 2017; Piasecki et al., 2018), decipher the intramolecular isotope equilibrium in natural system (Liu et al., 2019; Xie et al., 2020), identify the microbial activities in gas reservoirs (Gilbert et al., 2019), and so on. With the application of this new geochemical diagnostic tool, we can better constrain the gas history in the sedimentary basins. However, geological factors controlling the position-specific isotope of propane are not fully understood, for example the types of kerogen, which exerts a significant role on the intramolecular isotopic structures of the gaseous products. The characterization of PS isotope of propane generated from different types of source rock contributes to resolving this issue and identifying various geological processes in natural reservoirs. Marine shales and coals are the most important source rocks for the gas deposits in sedimentary basins worldwide. The latest study on the pyrolysis of the marine Woodford Shale

(Li et al., in review) has provided an insightful investigation on understanding the importance of kinetic and exchange reactions on chemical and isotopic compositions of gases produced in laboratory and natural conditions from the same source rock, and laying a framework of the generation of natural gases, and subsequent geochemical and microbial processes in natural reservoirs based on PS $\delta^{13}C$ and $\delta^{2}H$ isotopic compositions of propane.

Based on our previous work on the pyrolysis of immature Woodford Shale, here we conduct artificial maturation experiments on the Springfield coal with the aim to characterize the evolution of PS $\delta^{13}C$ from different kerogens, and interpreting the PS isotope compositions of propane in nature. The several methods for analyzing the position-specific isotope of propane have been developed: GC-pyrolysis-GC/IRMS (Gilbert et al., 2016), high-resolution mass spectrometry (Piasecki et al., 2016; Xie et al., 2018), GC/IRMS with chemical degradation (Gao et al., 2016) and quantitative nuclear magnetic resonance (qNMR) (Liu et al., 2018). In this study we apply an improved GC-pyrolysis-GC/IRMS technique (Li et al., in review) to accurately and precisely obtain the position-specific ^{13}C of propane. This study compares PS carbon isotopes of propane generated from different kerogen types or experienced secondary alternation to better constrain different geological processes in natural gas. Based on the bulk and position-specific isotopes of hydrocarbon gases generated from the gas-prone kerogen, we attempt to give an insightful look on the isotopic structure of kerogen that remains unresolved in modelling gas generation from the organic matter.

2 Samples and methods

A low maturity Pennsylvanian coal sample from the Illinois Basin used in this study was collected from the Oaktown mine in Springfield, Indiana. This coal has a total organic carbon (TOC) content

of 72.6%, H/C molar ratio of 0.93, vitrinite reflectance (%R_o) of 0.54, total sulfur content of 3.56%, oxygen content of 8.19%. The Springfield coal has $\delta^{13}C$ value of -25.4‰ of the kerogen fraction. The rock samples were collected fresh from a core, which was also used for the study of methane generation at low-temperature conditions (Wei et al., 2018). The coal was crushed into the size of 0.5 - 2 cm for the pyrolysis experiments.

2.1 Pyrolysis experiments

The experimental procedures in hydrous and anhydrous conditions were already described in details in Li et al. (in review). Hydrous pyrolysis experiments were conducted on the Springfield coal, using a ~ 300 ml bolted-closure Hastelloy reactor vessel at temperatures of 310, 340, 360 °C for 72 h each, 370 °C for 14 and 45 days. In general, 20 - 80 g samples and 60 - 80 g deionized water (DI) with δ^2H of -36 ± 0.2‰ were loaded into the quartz liner in the reactor, which was connected to a high-pressure 2-port valve via 1/16 inch stainless steel tubing. After checking for leak by pressuring the vessel with ~ 80 psi of air, the reactor was evacuated to 0.3 psi and placed in a convection oven. A K-type thermocouple, which was attached closely to the sample location of the reactor and wrapped by Al foil, was used to monitor the temperature in the reactor within ± 0.5 °C. Anhydrous pyrolysis experiments were conducted with the same Hastelloy vessel at 310, 340, 360, 380, 400, 415, 430, 450, 470 °C for 72 h each, without added DI water. After loading the samples into the liner, quartz wool was added to prevent the powders from contaminating or blocking the 1/4 inch tubes, when the reactor was evacuated to 0.1 torr. During the isothermal hydrous and anhydrous pyrolysis of the Springfield coal the reactor was heated to the target temperature in ~ 2 h, and cooled down to room temperature within ~ 1 h once the experiments were finished. In these series of pyrolysis experiments, the equivalent maturities for the temperature-time conditions were determined according to Sweeny and Burnham (1990).

After the pyrolysis experiments cooled dowm, the gaseous products in the headspace were collected by expanding the gas from the reactor to a pre-evacuated and calibrated volume connected to a pressure gauge. The total amounts of the gas were calculated based on the temperature and pressure according to the idea gas law. The gases were extracted by a 10-ml syringe through a septum, and stored in 10 ml pre-evacuated serum vials for the analysis of gas compositions, bulk isotope compositions, and position-specific ^{13}C isotope of propane.

2.2 Gas compositional and isotopic analysis

Gaseous and isotopic compositions of the gases from the pyrolysis of the Springfield coal were analyzed, using a gas chromatography-combustion/pyrolysis-isotope ratio mass spectrometry (GC-C/Py-IRMS). The gases stored in the serum bottles were injected by a gas-tight syringe and transferred by high-purity helium into a GC column CP7551 (HP-PLOT-Q, 27.5 m × 0.32 mm i.d. including 2.5 m particle trap, 10 μm film thickness), which was connected to GC Isolink and Finnigan Delta V plus mass spectrometer. The injector temperature was set at 100 °C with a split ratio of 8. The GC oven temperature was initially kept at 30 °C for 4 min and increased to 100 °C at a heating rate of 6 °C/min, followed by the increase to 220 °C at a heating rate of 20 °C, and then kept constant for 2 min. For bulk carbon isotope analysis, ~ 12 μl of the gas samples were injected and the combustion furnace temperature was set at 1030 °C with helium flow was 1.2 ml/min. For hydrogen isotopic composition, at least 25 μl gas samples were injected with the HTC temperature set at 1420 °C and the helium flow of 1 ml/min.

The chemical compositions of gaseous products (hydrocarbon gases, CO_2, H_2, H_2S) in the pyrolysis experiments were calibrated with a standard hydrocarbon gas mixture (Scotty Analyzed Gases), pure H_2 or CO_2 gas, a gas mixture of H_2S (1% mole concentration) balanced with N_2. The bulk carbon and hydrogen isotopic compositions were calibrated against the VPDB and VSMOW

scales, respectively using the natural gas standards obtained from USGS (Dias et al., 2016). The precisions of $\delta^{13}C$ and $\delta^{2}H$ are within ± 0.5‰ and ± 5‰ respectively (1 σ).

2.3 Position-specific carbon isotope analysis of propane

For the determination of intramolecular $\delta^{13}C$ values of propane in the pyrolysis gases, an improved GC-Pyrolysis-GC/IRMS method was described in Li et al. (in review). The key parameters for the measurements were summarized below. For the measurements of intramolecular $\delta^{13}C$ values of propane, approximately 60 ul gas samples with C_3H_8 contents of ~ 5% were injected via a gas-tight syringe and the injector temperature was at 100 °C using the split liner with the split ratio of 4. A first GC column (HP-PLOT-Q, 27.5 m × 0.32 mm i.d. including 2.5 m particle trap, 10 μm film thickness) separates the propane from samples. The gases were carried by high purity helium at 2.5 ml/min, into a high temperature pyrolysis furnace connected with a second column (CP-PoraPLOT-Q, 27.5 m × 0.32 mm i.d., 10 μm film thickness) to separate the CH_4, C_2H_4 and C_2H_6 fragments from propane cracking. The temperature of pyrolysis furnace was set at 800 - 820 °C. The temperature program in the first GC column was set: initially stayed at 50 °C for 15 min, then increased to 100 °C at 10 °C/min and held it for 10 min, and finally heated at 20 °C/min to 150 °C where it was kept for 15 min. The second column was placed in an oven and the temperature was kept at 25 °C during the measurements and increased to 180 °C after each measurement in order to elute the other longer-chain HCs retained in the column. After the correction for isotope fractionations associated with propane cracking to the fragments (Li et al., in review), accurate $\delta^{13}C$ values of terminal and central sites were obtained.

3 Results

3.1 Gas yields

In the hydrous and anhydrous pyrolysis of the Springfield coal, the gas molar yields (C_1-C_5, CO_2, H_2S and H_2) normalized to the TOC value, were shown as a function of the thermal maturities (Table 1, Fig. 1). The yields of methane, ethane, and propane generated in hydrous conditions increased from 0.15 to 1.85, 0.06 to 0.57, and 0.03 to 0.3 mmol/g TOC, respectively, at the Easy $\%R_o$ of 0.76 to 1.93. In the anhydrous pyrolysis experiments at maturity ranges from 0.76 to 3.07 %, methane yields increased from 0.13 to 5.55 mmol/g TOC, while ethane and propane yields increased continually with the maturities, followed by a decrease of their yields up to Easy $\%R_o$ of 3.07, due to the cracking of wet gas. The gas species of C_4 and C_5 as minor compositions of the pyrolysis gas showed increasing yields up to the Easy $\%R_o$ of 1.75 - 2, followed by the reduction due to the cracking reactions with increasing maturity. In this study the HC gases up to Easy $\%R_o$ of 2 were regarded as the products mainly sourced from thermal decomposition of kerogen and longer-chain HCs (C_{5+}), while at higher maturities the gases were mainly originated from the cracking of a mixture of the remained kerogen, wet-gas and other thermally stable organic compounds. As the most abundant non-hydrocarbon gases (Table 1), CO_2 yields in the hydrous conditions were much higher than those in the anhydrous conditions at the similar maturities mainly because of the interaction of water with carbonyl compounds in hydrous conditions (Lewan, 1997), which was similar to the observation of H_2S yields in the experiments with and without DI water. H_2S has various sources in the thermal maturation of coal, for instance thiols, sulfides and thiophenes (Lewan and Kotarba, 2014). The molar yields of H_2 in the hydrous conditions are comparable to the amounts in the anhydrous experiments, increasing from 0.01 to 0.13 mmol/g TOC at the Easy $\%R_o$ of 0.76 to 2, followed by a large increase up to 0.32 mmol/g TOC at the

highest maturity (Table 1). This implies that the H_2 is mainly sourced from organically bound hydrogen, as suggested by the open system pyrolysis of different types of source rocks showing the organic origin of H_2 (Li et al., 2015).

The molar yields of total hydrocarbon gases (C_1-C_5) increased significantly from 0.24 to 2.9 and from 0.23 to 6.15 mmol/g TOC in the hydrous and anhydrous experiments, respectively (Fig. 2). The gas dryness (C_1/(C_1-C_5)) in the pyrolysis experiments firstly decreased with the thermal maturity, and then increased continually with the highest values of 0.9 at Easy %R_o of 3.07 (Fig. 2). Such patterns of the evolution of gas dryness were also observed in the closed-system pyrolysis of immature Jurassic coal, extracted coal, and bitumen-rich coal at a heating rate of 2 or 20 °C/h (Li et al., 2013), and immature Cretaceous Cameo coal from the Piceance Basin (Zhang et al., 2008). This reflects that the gas produced at the early stage of coal cracking is relatively wet during the bond cleavage of various bonds (C-O, C-S, C-C).

3.2 Bulk isotopic compositions of hydrocarbon gases

As presented in Fig. 3 and Table 2, $\delta^{13}C$ values of C_1-C_3 in the hydrous and anhydrous pyrolysis experiments are similar at the similar maturities (Easy %R_o: 0.76 - 2), with the initial values of ~ -35, -29.5 and -29‰ at 310 °C. With increasing thermal maturation their highest $\delta^{13}C$ values were -31.5, -20.2 and 2.1‰, respectively, at 470 °C (Easy %R_o: 3.07). Previous studies on the hydrous pyrolysis of the Springfield coal with the same original $\delta^{13}C$ of kerogen (-25.4‰) as in this study, showed $\delta^{13}C$ values of CH_4 increased from ~ -57‰ to -44‰ with the increase of temperature from 60 to 200 °C for different time (6 - 24 months) (Wei et al., 2018). This is likely attributed to the temperature-dependent kinetic isotope effect in gas generation. The decrease of $\delta^{13}C_1$, and the relative constant values of $\delta^{13}C_2$ and $\delta^{13}C_3$ during coal kerogen cracking in this study were also observed in the closed-system pyrolysis of an immature Jurassic coal at 20 °C/h (Li et al., 2013)

and an immature Late Tertiary lignite at 10 °C/h (He et al., 2018). This can be explained by the cracking of various bonds associated to different $\delta^{13}C$ values in the gas precursors (Tang et al., 2000).

The δ^2H of C_1-C_3 in the anhydrous conditions showed heavier values than those in the hydrous pyrolysis experiments at similar maturities, indicating H from water is involved in the gas generation reactions (Fig. 3). With the added DI water (δ^2H: -36 ± 0.2‰) δ^2H_{C1} in the hydrous experiments at Easy $\%R_o$: 0.76 - 1.93 remained around -290‰, while those from the anhydrous conditions at Easy $\%R_o$: 0.76 - 3.07 kept increasing from -282 to -174‰. Low-temperature pyrolysis study verified that hydrogen from water has insignificant effect of δ^2H of CH_4, whereas for the pyrolysis experiments at high temperature ~ 50% of H in CH_4 was derived from water (Wei et al., 2018). Previous hydrous pyrolysis study on the Springfield coal at 60 - 200 °C showed δ^2H_{C1} values varying between -218 and -275‰ with δ^2H_{H2O} of -137 or 1246‰ (Wei et al., 2018), which are similar to the variations of δ^2H_{C1} in the anhydrous pyrolysis in this study (310 to 400 °C). This indicated that the physical and chemical properties of water related to the temperature also plays an important factor in influencing the δ^2H in the pyrolysis conditions, besides the H KIE.

3.3 Position-specific C isotopes of propane

In the hydrous and anhydrous pyrolysis of the Springfield coal the position-specific carbon isotope deviation ($\Delta C_{c\text{-}t} = \delta^{13}C_{cen} - \delta^{13}C_{ter}$) changed from 3.2 ± 1.2 to 22.7 ± 1.2‰ in the entire maturity range of 0.76 to 3.07 with a significant increase at the Easy $\%R_o$ above 2 (Fig. 4). The variations of $\Delta C_{c\text{-}t}$ values in this study closely matched the results from the hydrous and anhydrous pyrolysis of the immature marine Woodford shale (Li et al., in review), indicating that maturity is a significant factor in controlling the $\Delta C_{c\text{-}t}$. Compared with the values of $\Delta C_{c\text{-}t}$ in equilibrium state (Webb and Miller, 2014) within the temperature range of ~ 27 to 327 °C, our results showed that

the propane generated in the pyrolysis conditions (310 to 470 °C) were not in equilibrium, indicating the position-specific C isotopes were mainly controlled by the kinetic processes. The larger increases of $\Delta C_{c\text{-}t}$ values in the pyrolysis of coal compared with those from the cracking of single compound of n-C_{25} and C_3H_8 were observed at the wet gas cracking stage (Fig. 4).

The $\delta^{13}C$ values at the terminal and central positions of propane increased from ~ -30 ± 0.5 to -5.3 ± 0.5‰, and from ~ -26.5 ± 1.1 to 17.4 ± 1.1‰, respectively with the significant increases at Easy %R_o above 2 (Table 3 and Fig. 5). The $\delta^{13}C$ at the central position was heavier than that in the terminal position, which was also observed in closed-system pyrolysis of the Woodford shale (Li et al., in review) and natural thermogenic propane (Gao et al., 2016; Liu et al., 2019) or biodegraded propane (Gilbert et al., 2019). In the hydrous and anhydrous conditions at the similar maturities, the values of $\delta^{13}C_{ter}$ or $\delta^{13}C_{cen}$ are close, indicating the similar propane generation processes.

3.4 Kinetic isotope effect in gas generation

The bulk and position-specific carbon isotope fractionation of hydrocarbon gases have been verified to be associated with the kinetic isotope effect (KIE) in the cleavage of various bonds (e.g., C-C, C-S, C-O) attached to different functional groups. Assuming gas generation follows the Rayleigh model at the initial kerogen cracking (310 °C, Easy %R_o: 0.76) (Li et al., in review), the KIE was calculated based on the original $\delta^{13}C$ of the Springfield coal, and kinetic parameters of gas generation and cracking in the pyrolysis experiments (Zhang et al., 2008; Li et al., 2021) (Fig. 6). At the initial stage of coal kerogen cracking, the carbon isotope fractionation factors (α) of CH_4 in the hydrous and anhydrous conditions were 0.9900 ± 0.0007 and 0.9894 ± 0.0007, respectively, with the values of 0.9957 ± 0.0007 and 0.9955 ± 0.0007 for C_2H_6, and the values of 0.9962 ± 0.0007 and 0.9964 ± 0.0007 for C_3H_8. The isotope fractionations were larger than those of C_1-C_3

generated in the pyrolysis of xylite in the high temperature conditions (450 ºC) (Berner et al., 1995). The CH_4 KIE in this study at 310 ºC was much smaller compared with that in the pyrolysis of the Springfield coal at low temperature (0.9674 at 60 ºC, 0.9807 at 200 ºC) (Wei et al., 2018). In the wet-gas cracking stage the KIE of C_3H_8 in this study was significantly lower than those from the immature marine Woodford kerogen (Fig. 6) at the same temperature conditions (Li et al., in review).

The α values for carbon at the terminal and central sites of propane in the pyrolysis of the Springfield coal at 310 ºC were 0.9952 ± 0.0007 and 0.9985 ± 0.0007 in the hydrous experiments, similar to the anhydrous conditions: 0.9953 ± 0.0007 and 0.9989 ± 0.0007, respectively. The relatively larger isotope fractionation in the terminal site was also observed in the pyrolysis of the Woodford Shale (Li et al., in review) and theoretical model (Tang et al., 2000) (Fig. 7). In C_3H_8 cracking, the carbon isotope fractionation at the terminal and central sites of propane in the pyrolysis of the Springfield coal were smaller than those in the Woodford Shale maturation at the temperature range of 430 - 480 ºC (Fig. 7), but exceeded greatly those in pure propane cracking (Li et al., 2021).

4 Discussion

4.1 Hydrocarbon gas generation and propane cracking

The Springfield coal in this study has a thermal maturity equivalent to vitrinite reflectance of 0.54%, a TOC value of 72.6% and H/C ratio of 0.93, which show similar geochemical characterization as the immature Cameo coal in the Piceance Basin (0.5%, 77% and 0.9, respectively) (Zhang et al., 2008). The maceral composition of the Springfield coal is 85% vitrinite,

2.9% liptinite and 12.1% inertinite, which is relatively close to the petrographic composition of the Cameo coal (87.2%, 4.6%, 8.2%, respectively). Therefore the Springfield coal is geochemically and petrographically similar to the Cameo coal, which makes it reliable to use the kinetic parameters from the latter to model the thermogenic gas generation in this study. This is likely one of the reasons why the experimental gas dryness for the two samples at different temperature conditions are similar at Easy $\%R_o$ above 1.4 (Fig. 2).

In the pyrolysis of the Springfield coal, hydrocarbon gas generation and wet-gas cracking are compared with kinetic models (Fig. 1) based on several parallel, first-order reactions with a distribution of activation energies (E_a) due to the high heterogeneities of chemical structures of coal (e.g., Burnham et al., 1987; Tang et al., 1996). The kinetic parameters obtained from the pyrolysis studies involved in the reactions prior to secondary cracking ($\%R_o$ < ~ 2.2) (Hill et al., 2007; Zhang et al., 2008) are used to calculate the hydrocarbon gas yields at the maturity range of Easy $\%R_o$ of 0.76 to ~ 2 in this study. In this calculation the maximum amounts of CH_4, C_2H_6 and C_3H_8 are assumed to be 100%, 20% and 20% higher than the experimental gas yields at Easy $\%R_o$ of ~2, based on Zhang et al. (2008). The maximum total gas amounts is assumed to be 50% higher than the measured results at Easy $\%R_o$ up to 2, based on the gas amount applied for the determination of kinetic parameters in the pyrolysis of immature Barnett Shale (Hill et al., 2007). As shown in Fig. 1, the CH_4 yields are slightly larger than the prediction from kinetic model on the pyrolysis of immature Cameo coal (Zhang et al., 2008), but lower than those from kinetic calculation based on the early CH_4 generation from the Tertiary lignite (Tang et al., 1996). The yields of C_2H_6 and C_3H_8 are close to the calculated amount based on the kinetic model (Zhang et al., 2008). The lignite used in the previous pyrolysis experiments (Tang et al., 1996) has a $\%R_o$ of 0.31, a TOC value of 61.2% and H/C ratio of 0.78, with the maceral composition of 91% vitrinite,

5% liptinite and 4% inertinite. Possibly the maturity difference between the Springfield coal and lignite plays a significant role in the discrepancy of CH_4 yields.

During the wet gas cracking (Easy $\%R_o$ > 2) C_3H_8 yields in this study is compared with the theoretical calculation based on the pure propane cracking (Tian et al., 2008; Li et al., 2021) and the immature Woodford Shale (Li et al., in review), with maximum C_3H_8 amounts 5% higher than the measured yields at Easy $\%R_o$ of 2. Our experimental results agree with the calculated C_3H_8 yields by kinetic parameters from the pure propane cracking (Fig. 1), but present lower values than those based on the Woodford Shale pyrolysis where significant amount of C_3H_8 are produced at high maturity stage. This indicates that in the pyrolysis of coal C_3H_8 generation potential at high maturity stage is limited, possibly as a byproduct in aromatization/polymerization of the remaining kerogen. The discrepancy in C_3H_8 yields between the two kerogens suggest that oil/secondary cracking to C_3H_8 during the wet-gas cracking plays an important role in the marine Woodford kerogen, as indicated by the comparison of gas generation from type II and III kerogens (Behar et al., 1995). The total gas yields (C_1-C_5) at Easy $\%R_o$ of 0.76 to 2 modeled by the kinetic parameters based on the anhydrous pyrolysis of immature marine Barnett Shale (Hill et al., 2007) match the experimental results in the anhydrous conditions, but deviate slightly from those in the hydrous pyrolysis. The marine Barnett Shale has a $\%R_o$ of 0.44, TOC of 5.5% and H/C ratio of 1.4, which has similar maturity to the Springfield coal. Although the two kerogen have different chemical structures, the immature Springfield coal and Barnett Shale have similar gas generation potentials in the maturity range before the wet gas cracking.

The extrapolation of kinetic parameters obtained in the high-temperature conditions to natural reservoirs could lead to a large underestimation of gas yields, as indicated by a recent study on the low-temperature pyrolysis of marine New Albany Shale (Wei et al., 2018). Here, we apply kinetic

parameters based on the pyrolysis experiments from 280 to 490 °C (Zhang et al., 2008) to calculate the CH_4 yields at the temperature range of 60 - 200 °C for 6 - 12 months in the previous study (Wei et al., 2018). The predicted results are 6 - 9 orders of magnitude lower than the CH_4 yields in the low-temperature pyrolysis of the Springfield coal, indicating the gas generation from coal is also largely underestimated in natural reservoirs by extrapolating the kinetic data from high-temperature pyrolysis experiments, as observed in marine New Albany Shale (Wei et al., 2018).

4.2 Kinetic isotope effect in gas generation

In this section, we explore what influences the PS C isotope of propane in the thermal maturation of organic matter as well as kinetic isotope effect, and interpret the PS isotopes in the gas generation from the Springfield coal as well as explore the isotopic structures of kerogen.

4.2.1 Bulk isotope effect of C_1-C_3

A comparison of kinetic isotope effects of C_1-C_3 generation and C_3H_8 cracking in the pyrolysis of the Springfield coal at temperature of 310 to 470 °C with those from the pyrolysis of the Springfield coal at 60 - 200 °C (Wei et al., 2018), the Woodford Shale (Li et al., in review) and C_3H_8 (Li et al., 2021), and theoretical models on gas generation from the cracking of n-alkane ($\leq C_6$) (Tang et al., 2000), n-C_8 (Ni et al., 2011) is presented (Fig. 6). The carbon isotope fractionation is much larger for methane generation at low temperatures compared with those in this study due to the temperature-dependent KIE. Because of the heterogeneity of gas precursors and multiple sources, the C isotope fractionation in the pyrolysis of marine kerogen and coal does not match the prediction from the cracking of n-alkane (Tang et al., 2000). In the wet-gas cracking stage the carbon KIE in this study is not as large as those observed in the pyrolysis of marine Woodford kerogen, but much larger than those in the pure propane cracking, possibly due to different propane generation potentials at high maturity as indicated in Li et al. (in review). The previous pyrolysis

studies on mature coals verify the low C_3H_8 yields at the wet-gas cracking (Lewan and Kotarba, 2014; Li et al., 2018). This is supported by the pyrolysis of mature type II and III kerogen with $\%R_o$ of 1.4 and 1.3, respectively, showing the C_3H_8 yields are ~ 2 times larger in marine shale than those of coal in the pyrolysis experiments at 400 °C for 24 h and 450 °C for 3 h (Lorant and Behar, 2002).

To interpret the decrease of $\delta^{13}C_1$ with increasing thermal maturity, we assume $\delta^{13}C$ of the gas precursors is the same as value of kerogen (-25.4‰) in gas generation. Due to the lower dissociation energy of hetero bonds, HC gases are formed by the cracking of C-S/C-O bonds first, rather than C-C, during the maturation of coal. The C KIE associated with the C-O breaking for CH_3- radical attached to aromatics is smaller (~ 0.9901) than those of C-C (~ 0.9847) at 310 °C (Tang et al., 2000). CH_4 produced from C-O cracking of the kerogen at low maturity (Easy $\%R_o$: 0.76) would have a $\delta^{13}C_1$ value of ~ 35.3‰, which is close to the observed values in the pyrolysis of Springfield coal (Fig. 3). With increasing maturity, C-C cracking increasingly produces C_1-C_3 with larger C KIE and lower $\delta^{13}C$ values, consistent with the observations of the $\delta^{13}C_1$ in the pyrolysis gases. The C KIE for C-O cleavage is 0.9619 at 60 °C and 0.9813 at 200 °C, which results in the $\delta^{13}C_1$ values of ~ 63 and ~ 44‰, respectively. This calculation matches the $\delta^{13}C_1$ in the pyrolysis of Springfield coal at 200 °C, and presents more negative value (by 6‰) than that at 60 °C (Wei et al., 2018). This further confirms that the CH_4 is sourced from the C-O bonds cracking at early maturation. At the lowest temperature (60 °C) for 6 - 12 months, the relatively heavy experimental $\delta^{13}C_1$ possibly implies CH_4 is produced from the mixtures of C-S and C-O bonds cleavage, as suggested by the smaller C KIE of 0.9732 at 60 °C in breaking C-S bonds (Tang et al. 2000). Based on the S and O contents in the kerogen of the Springfield coal (2.8 and 8.3%, respectively), the amounts of C-O bonds are approximately 6 times more than those of C-S bonds

in this coal assuming both S and O exist in the form of single bond. Combined with the $\delta^{13}C_1$ of ~ -57‰ in the pyrolysis of the Springfield coal at 60 °C (Wei et al., 2018), isotope balance calculation suggests 44% of CH_4 is produced from the cracking of C-O bond while 56% is sourced from the C-S bond cleavage. The C KIE of C_2H_6 and C_3H_8 generated from C-C cracking are 0.9926 and 0.9930 at 310 °C (Tang et al., 2000), respective, leading to their $\delta^{13}C$ values more negative by ~ 3‰ than the measured values. This indicates C_2H_6 and C_3H_8 are likely to be also produced by the cleavage of hetero bonds with relatively small C KIE at early stages of coal kerogen.

4.2.2 Position-specific isotope effect of propane

This study compares the position-specific C KIE of propane sourced from the marine Woodford Shale, Springfield coal and single organic compound at different temperatures (Fig. 7). The smaller fractionation at the terminal and central site of propane produced in the pyrolysis of the Springfield coal compared with those in the Woodford Shale at the same temperature (310 °C) (Li et al., in review) and theoretical model (Tang et al., 2000) indicates the difference of bonds cleavage at an early gas generation stage, as observed in the bulk C KIE (Fig. 6). Coal is more enriched in heteroatom-compounds (e.g., O, S) and aromatics structures, compared with the marine kerogen. The C KIE of propyl groups cleaved from C-O bonds could be smaller than those from C-C bonds, as suggested by the fractionation factors for the cracking of methyl radicals from various organic structures (Tang et al., 2000). Therefore, the propyl radicals attached to the hetero compounds in coal could be main factor that results in the relatively small position-specific C KIE at early propane generation. The position-specific isotope fractionation at the initial Woodford kerogen cracking matches the theoretical calculation based on propyl groups cleaved from n-alkanes ($n \leq 6$) (Tang et al., 2000), indicating the C-C bonds cleavage in the aromatics occurring at the terminal site is likely the main propane generation pathways.

During propane cracking in this study the isotope fractionation in the central position is larger than that in the terminal position, as observed in the pyrolysis of Woodford Shale (Li et al., in review). The difference of the position-specific isotope fractionation of propane between the two kerogens is consistent with the observation of bulk C KIE (Fig. 6). Together with the comparison of C_3H_8 yields in the cracking of Woodford kerogen, Springfield coal and C_3H_8 (Fig. 1), and bulk C KIE (Fig. 6), the different C_3H_8 generation potentials during the wet-gas cracking stage is the main factor leading to the different magnitude of position-specific C KIE (Li et al., in review).

4.2.3 Position-specific $\delta^{13}C$ deviation of propane and isotopic structures of kerogen

At high maturity stage (Easy $\%R_o > 2$), significant increases of $\Delta C_{c\text{-}t}$ with the maturity in the both Springfield coal and Woodford Shale were observed, but the pure propane cracking will not lead to such a large increase in the $\Delta C_{c\text{-}t}$ (Li et al., 2021). We compare the $\Delta C_{c\text{-}t}$ values of propane in the pyrolysis of the Woodford Shale, Springfield coal, and C_3H_8, with those from the kinetic Monte Carlo (kMC) simulations on the cracking of n-alkane compound ($n\text{-}C_{40}/n\text{-}C_{20}$) (Petersons et al., 2018) (Fig. A1). We have normalized their simulation results with the initial $\delta^{13}C$ values of the alkanes same as that of the Springfield coal (-25.4‰). The increase of $\Delta C_{c\text{-}t}$ during the pyrolysis of the Springfield coal is consistent with late-stage production of C_3H_8 from nC_{20}/nC_{40} in the kMC simulations, which is also observed in the Woodford pyrolysis study (Li et al., in review). The larger magnitude of $\Delta C_{c\text{-}t}$ of propane in the kMC simulations could be likely due to the random distribution of ^{13}C in the substrates, significant kinetic isotope fractionation (-30‰) for C-C bonds cracking, and no consideration of secondary/tertiary isotope effects. This also implies that propyl groups ($CH_3\text{-}CH_2\text{-}CH_2\text{-}$) of the Woodford Shale and Springfield coal have non-random distributions of ^{13}C in kerogen, as indicated by the heterogeneity of the terminal three C of long-chain n-alkanes varying by ~ 12‰ (Gilbert et al., 2013).

Currently we have little insight into the isotopic structures of kerogens in sedimentary basins, a major obstacle for understanding the kinetic processes and predicting the geochemical characterization of hydrocarbon products. In the modelling of the specific isotopologues of hydrocarbon gases generated from organic compounds, it is assumed that the internal isotope distributions within the precursors are homogeneous (e.g., Tang et al., 2000; Petersons et al., 2018). A potential way to tackle this issue is to analyze the isotopic structures of gaseous compounds generated from the thermal maturation of kerogen. The difference of $\delta^{13}C$ between the humic and marine kerogen is around 3.6‰, which is smaller than that of $\delta^{13}C_3$ of the two kerogens at the same temperature (e.g., 6.5‰ at 310 °C). This suggests the bond types that propyl groups attach to other radicals are different in the Springfield coal and Woodford Shale, leading to the various KIE. Theoretical calculation on the cleavage of propyl groups at the terminal position from the C-C bonds (Tang et al., 2000) agrees well with the $\delta^{13}C_3$ of ~ -36‰ in the Woodford Shale at 310 °C, but presents more negative value (-32.4‰) than that in the Springfield coal (-29‰). This indicates propyl groups attached to the hetero compounds are relatively widespread in the humic kerogen due to the smaller KIE in the cracking of C-O and C-S bonds (Tang et al., 2000), while the propyl radicals mainly exist in the form of C-C bonds in the marine kerogen.

The similar trend of $\delta^{13}C_{ter}$ and $\delta^{13}C_{cen}$ of propane with increasing maturity in the pyrolysis of both humic and marine kerogens (Fig. A2) and the agreements of position-specific C KIE in the Woodford Shale with theoretical modelling on the propyl radicals cleavage from n-alkane at 310 °C (Tang et al., 2000) (Fig. 7), indicate the bond cracking possibly occurs at the terminal site of the propyl groups and the bond cleavage from hetero compounds are the main source of propane at an early cracking stage in coal. The continual increase of $\delta^{13}C_{cen}$ with increasing maturity at kerogen cracking stage, which surpasses the constant $\delta^{13}C_{ter}$, suggests the ^{13}C values at the central

site of propyl groups are possibly heavier than those at the terminal sites in both humic and marine kerogens. The increase of $\delta^{13}C_{ter}$ at Easy $\%R_o$ from 0.76 to ~ 2 in the Springfield coal is less significant than those in the Woodford Shale, implying the ^{13}C at the terminal site of propyl radicals attached to different functional groups is likely more heterogeneous within humic kerogen. The insights into intramolecular ^{13}C of propyl groups also suggest the non-random isotope distribution within kerogen, as indicated in the comparison of $\Delta C_{c\text{-}t}$ values from the kMC simulation and gas-prone kerogens (Fig. A1).

4.3 Insights into the propane history in natural reservoirs

In coal maturation gas generation is associated with the elimination of oxygenated functional groups with low oil potential (Behar and Vandenbroucke, 1987), during which the propane precursors are shifted from the hetero compounds to the alkyl structures. The influence of formation processes, and subsequent geochemical and microbial activities on the position-specific $\delta^{13}C$ and $\delta^{2}H$ of propane in natural reservoirs has been discussed (Li et al., in review). Here we extend this framework to summarize the $\delta^{13}C_{ter}$ and $\delta^{13}C_{cen}$ of propane from this study, pyrolysis gases from the Woodford Shale, and pure n-C_{25} and C_3H_8, natural gas samples, and kMC simulations of propane generation from n-C_{40}/n-C_{20} (Piasecki et al., 2018; Gilbert et al., 2019; Liu et al., 2019; Zhao et al., 2020; Li et al., 2021; Li et al., in review) (Fig. 8). In the pyrolysis gases and most of natural gas samples the $\delta^{13}C_{ter}$ values are lower than $\delta^{13}C_{cen}$, suggesting the similar isotopic structures of propane precursors in the kerogen. In the most gas samples from natural and laboratory conditions, the intramolecular $\delta^{13}C$ values of propane are not in equilibrium, possibly due to the much longer time required for C isotope equilibria, compared with intramolecular $\delta^{2}H$ values, which show equilibrium state in Eagle Ford Shale gas (Xie et al., 2020). Biodegradation appears to have more significant effect on the $\delta^{13}C_{cen}$ than the $\delta^{13}C_{ter}$, as indicated in the U.

Devonian Antrim reservoir (Gilbert et al., 2019). The abiogenic origin of a gas sample from a terrestrial serpentine-hosted hot spring (Suda et al., 2017) shows similar $\delta^{13}C_{ter}$ as the $\delta^{13}C_{cen}$, which is different from those in the thermogenic and biodegraded gases.

The stable isotopic compositions of HC gases have been commonly used to fingerprint natural gas origin in the sedimentary basins (e.g., Schoell, 1988; Milkov and Etiope, 2018). However, the complex geological processes could hinder effective identification. For example, the mixing of kerogen/oil cracking gas, wet-gas cracking gas leads to the wide ranges of chemical contents and carbon isotopes of ethane and propane in the Ordovician gases in the Tarim Basin (Liu et al., 2019). The abiogenic origin of natural gases in Kidd Creek Mine, Canada (Sherwood Lollar et al., 2002), can be misled as the coal-type thermogenic source based on the Bernard diagram ($C_1/(C_2+C_3)$ vs $\delta^{13}C_1$). The deep-gases in the Xujiaweizi Depression in the Songliao Basin, China, were previously considered as a mixture of abiotic and biotic gases, but have been verified to be purely thermogenic gases generated from high-mature coal ($\%R_o$: 2 - 4) and a marine kerogen ($\%R_o$: 1.2 - 3) (Shuai et al., 2018). The $\delta^{13}C_{ter}$ and $\delta^{13}C_{cen}$ values of propane could provide an additional dimension of geochemical information on the gas history, detecting different activities in the subsurface (e.g., thermal degradation, anaerobic or aerobic biodegradation) (Gilbert, 2021).

5 Conclusions

We examined the position-specific ^{13}C of propane generated from the pyrolysis of the Springfield coal compared with those from the marine Woodford Shale cracking (Li et al., in review). Hydrocarbon gases are generated from the cracking first of hetero compounds (e.g., C-O, C-S) and then alkyl groups during coal maturation, as suggested by wide distributions of activation energies

and the decrease of $\delta^{13}C_1$. At the wet-gas cracking stage (Easy $\%R_o > 2$) C_3H_8 production potential is a main factor influencing the C_3H_8 cracking rates, and isotope effect at bulk and position-specific levels in the pyrolysis of the gas-prone kerogen. The smaller C KIE at the terminal and central sites of propane at the early cracking of the Springfield coal compared with the marine Woodford Shale are mainly attributed to the different types of bonds cleavage in kerogen. The similar $\Delta C_{c\text{-}t}$ values of propane generated from the marine kerogen and the coal indicate that maturity is a main factor controlling the intramolecular $\delta^{13}C$ deviation, and that at wet-gas cracking stage C_3H_8 production from thermally stable compounds with relative heavy ^{13}C has a significant influence on the $\Delta C_{c\text{-}t}$ value as shown in the kMC simulation on n-alkane cracking (Peterson et al., 2018). The position-specific $\delta^{13}C$ values of propane produced at the kerogen cracking stage indicate the original ^{13}C at the central site of propyl groups is likely more positive than that at the terminal site. The $^{13}C_{ter}$ of the propyl radicals attached to various functional groups is more heterogeneous within the humic kerogen.

In the pyrolysis gases, including the marine Woodford Shale and Springfield coal, and most of natural gas samples, the $\delta^{13}C_{ter}$ is more negative than the $\delta^{13}C_{cen}$, suggesting similar isotopic structures of organic precursors in kerogen. Thermal cracking and biodegradation seem to have a more significant effect on the $\delta^{13}C_{cen}$ than the $\delta^{13}C_{ter}$ of propane, as observed in the laboratory pyrolysis gas, and natural gas from the U. Devonian Antrim deposit in the Michigan Basin, as well as propane production from the kMC simulation. The PS $\delta^{13}C$ values of propane from the Woodford Shale and Springfield coal indicate the potential to serve as a geochemical diagnostic tool for fingerprinting the gas origins in geological conditions (primary vs. secondary cracking). Further work on analyzing the PS isotopes of natural gas samples with a series of maturity gradient

from different types of source rocks, contributes to better constraining the gas history in natural reservoirs.

Acknowledgements

Financial support was provided by U. S. Department of Energy Geosciences program (DE-SC0016271).

Referneces

Behar, F., Vandenbroucke, M., 1987. Chemical modelling of kerogen. Organic Geochemistry 11, 15-24.

Behar, F., Vandenbroucke, M., Teermann, S.C., Hatcher, P.G., Leblond, C., Lerat, O., 1995. Experimental simulation of gas generation from coals and a marine kerogen. Chemical Geology 126, 247-260.

Berner, U., Faber, E., Scheeder, G., Panten, D., 1995. Primary cracking of algal and landplant kerogens: kinetic models of isotope variations in methane, ethane and propane. Chemical Geology 126, 233-245.

Burnham, A.K., Braun, R.L., Gregg, H.R., Samoun, A.M., 1987. Comparison of methods for measuring kerogen pyrolysis rates and fitting kinetic parameters. Energy & Fuels 1, 452-458.

493 Dias, R., Ellis, G., Coleman, D., 2016. Development and calibration of new natural gas d13C and
494 d2H reference standards. International Conference and Exhibition, Barcelona, Spain, 3-6 April
495 2016. Society of Exploration Geophysicists and American Associate of Petroleum Geologists,
496 228.

497 Gao, L., He, P.Q., Jin, Y.B., Zhang, Y.Q., Wang, X.Q., Zhang, S.C., Tang, Y.C., 2016.
498 Determination of position-specific carbon isotope ratios in propane from hydrocarbon gas
499 mixtures. Chemical Geology 435, 1-9.

500 Gilbert, A., Yamada, K., Yoshida, N., 2013. Exploration of intramolecular ^{13}C isotope
501 distribution in long chain n-alkanes (C11-C31) using isotopic ^{13}C NMR. Organic
502 Geochemistry 62, 56-61.

503 Gilbert, A., Yamada, K., Suda, K., Ueno, Y., Yoshida, N., 2016. Measurement of position-specific
504 ^{13}C isotopic composition of propane at the nanomole level. Geochimica et Cosmochimica Acta
505 177, 205-216.

506 Gilbert, A., Lollar, B.S., Musat, F., Giunta, T., Chen, S.C., Kajimoto, Y., Yamada, K., Boreham,
507 C.J., Yoshida, N., Ueno, Y., 2019. Intramolecular isotopic evidence for bacterial oxidation of
508 propane in subsurface natural gas reservoirs. Proceedings of the National Academy of Sciences
509 116, 6653-6658.

510 Gilbert, A., 2021. The organic isotopologue frontier. Annual Review of Earth and Planetary
511 Sciences 49, 435-464.

512 He, K., Zhang, S.C., Mi, J.K., Zhang, W.L., 2018. The evolution of chemical groups and
513 fractionation at different maturation stages during lignite pyrolysis. Fuel 211, 492-506.

514 Hill, R.J., Zhang, E., Katz, B.J., Tang, Y.C., 2007. Modeling of gas generation from the Barnett
515 Shale, Fort Worth Basin, Texas. AAPG Bulletin 91, 501-521.

516 Lewan, M.D., 1997. Experiments on the role of water in petroleum formation. Geochimica et
517 Cosmochimica Acta 61, 3691-3723.

518 Lewan, M.D., Kotarba, M.J., 2014. Thermal-maturity limit for primary thermogenic-gas
519 generation from humic coals as determined by hydrous pyrolysis. AAPG Bulletin 98, 2581-
520 2610.

521 Li, E.T., Pan, C.C., Yu, S., Jin, X.D., Liu, J.Z., 2013. Hydrocarbon generation from coal, extracted
522 coal and bitumen rich coal in confined pyrolysis experiments. Organic Geochemistry 64, 58-
523 75.

524 Li, X.Q., Krooss, B.M., Weniger, P., Littke, R., 2015. Liberation of molecular hydrogen (H_2) and
525 methane (CH_4) during non-isothermal pyrolysis of shales and coals: Systematics and
526 quantification. International Journal of Coal Geology 137, 152-164.

527 Li, X.Q., McGovern, G.P., Horita, J., 2021. Kinetics of propane cracking and position-specific
528 isotope fractionation: Insights into the origins of natural gases. Organic Geochemistry 155,
529 104234.

530 Li, X.Q., Horita, J. Molecular and intramolecular isotope study on natural and laboratory
531 generation of thermogenic gases from the Woodford Shale. Geochimica et Cosmochimica Acta
532 (in review).

533 Li, W., Zhu, Y.M., Liu, Y., 2018. Gas evolution and isotopic fractionation during pyrolysis on coals
534 of different ranks. International Journal of Coal Geology 188, 136-144.

Liu, C.J., McGovern, G.P., Liu, P., Zhao, H., Horita, J., 2018. Position-specific carbon and hydrogen isotopic compositions of propane from natural gases with quantitative NMR. Chemical Geology 491, 14-26.

Liu, C.J., Liu, P., McGovern, G.P., Horita, J., 2019. Molecular and intramolecular isotope geochemistry of natural gases from the Woodford Shale, Arkoma Basin, Oklahoma. Geochimica et Cosmochimica Acta 255, 188-204.

Liu, Q.Y., Wu, X.Q., Wang, X.F., Jin, Z.J., Zhu, D.Y., Meng, Q.Q., Huang, S.P., Liu, J.Y., Fu, Q., 2019. Carbon and hydrogen isotopes of methane, ethane, and propane: A review of genetic identification of natural gas. Earth-Science Reviews 190, 247-272.

Lorant, F., Behar, F., 2002. Late generation of methane from mature kerogens. Energy & Fuels 16, 412-427.

Milkov, A.V., Etiope, G., 2018. Revised genetic diagrams for natural gases based on a global dataset of > 20,000 samples. Organic Geochemistry 125, 109-120.

Ni, Y.Y., Ma, Q.S., Ellis, G.S., Dai, J.X., Katz, B., Zhang, S.C., Tang, Y.C., 2011. Fundamental studies on kinetics isotope effect (KIE) of hydrogen isotope fractionation in natural gas systems. Geochimica et Cosmochimica Acta 75, 2696-2707.

Peterson, B.K., Formolo, M.J., Lawson, M., 2018. Molecular and detailed isotopic structures of petroleum: Kinetic Monte Carlo analysis of alkane cracking. Geochimica et Cosmochimica Acta 243, 169-185.

Piasecki, A., Sessions, A., Lawson, M., Ferreira, A.A., Neto Santos, E.V., Eiler, J.M., 2016. Analysis of the site-specific carbon isotope composition of propane by gas source isotope ratio mass spectrometer. Geochimica et Cosmochimica Acta 188, 58-72.

557 Piasecki, A., Sessions, A., Lawson, M., Ferreira, A.A., Neto Santos, E.V., Ellis, G.S., Lewan, M.D.,
558 Eiler, J.M., 2018. Position-specific ^{13}C distributions within propane from experiments and
559 natural gas samples. Geochimica et Cosmochimica Acta 220, 110-124.

560 Schoell, M., 1988. Multiple origins of methane in the earth. Chemical Geology 71, 1-10.

561 Sherwood Lollar, B., Westgate, T.D., Ward, J.A., Slater, G.F., Lacrampe-Couloume, G., 2002.
562 Abiogenic formation of alkanes in the Earths crust as a minor source for global hydrocarbon
563 reservoirs. Nature 416, 522-524.

564 Shuai, Y.H., Etiope, G., Zhang, S.C., Douglas, P.M.J., Huang, L., Eiler, J. M., 2018. Methane
565 clumped isotopes in the Songliao Basin (China): Nedw insights into abiotic vs. biotic
566 hydrocarbon formation. Earth and Planetary Science Letters 482, 213-221.

567 Suda, K., Gilbert, A., Yamada, K., Yoshida, N., Ueno, Y., 2017. Compound- and position-specific
568 carbon isotopic signatures of abiogenic hydrocarbons from on-land serpentinite-hosted Hakuba
569 Happo hot spring in Japan. Geochimica et Cosmochimica Acta 206, 201-215.

570 Sweeney, J.J., Burnham, A.K., 1990. Evaluation of a simple model of vitrinite reflectance based
571 on chemical kinetics. AAPG Bulletin 74, 1559-1570.

572 Tang, Y.C., Jenden, P.D., Nigrini, A., Teerman, S.C., 1996. Modeling early methane generation
573 in coal. Energy & Fuels 10, 659-671.

574 Tang, Y., Perry, J.K., Jende, P.D., Schoell, M., 2000. Mathematical modeling of stable carbon
575 isotope ratios in natural gases. Geochimica et Cosmochimica Acta 64, 2673-2687.

576 Tian, H., Xiao, X.M., Wilkins, R.W.T, Tang, Y.C., 2008. New insights into the volume and
577 pressure changes during the thermal cracking of oil to gas in reservoirs: Implications for the in-
578 situ accumulation of gas cracked from oils. AAPG Bulletin 92, 181-200.

579 Wei, L., Schimmelmann, A., Mastalerz, M., Lahann, R.W., Sauer, P.E., Drobniak, A., Strąpoć, D.,
580 Mango, F.D., 2018. Catalytic generation of methane at 60 – 100 °C and 0.1 – 300 MPa from
581 source rocks containing kerogen Types I, II and III. Geochimica et Cosmochimica Acta 231,
582 88-116.

583 Xia, X.Y., Gao, Y.L., 2019. Kinetic clumped isotope fractionation during the thermal generation
584 and hydrogen exchange of methane. Geochimica et Cosmochimica Acta 248, 252-273.

585 Xie, H., Ponton, C., Formolo, M.J., Lawson, M., Peterson, B.K., Lloyd, M.K., Sessions, A.L., Eiler,
586 J.M., 2018. Position-specific hydrogen isotope equilibrium in propane. Geochimica et
587 Cosmochimica Acta 238, 193-207.

588 Xie, H., Ponton, C., Formolo, M.J., Lawson, M., Ellis, G.S., Lewan, M.D., Ferreira, A.A., Morais,
589 E.T., Spigolon, A.L.D., Sessions, A.L., Eiler, J.M., 2020. Position-specific distribution of
590 hydrogens in natural propane: Effects of thermal cracking, equilibration and biodegradation.
591 Geochimica et Cosmochimica Acta 290, 235-256.

592 Zhang, E., Hill, R.J., Katz, B.J., Tang, Y.C., 2008. Modeling of gas generation from the Cameo
593 coal zone in the Piceance Basin, Colorado. AAPG Bulletin 92, 1077-1106.

594

Fig. 1. Evolution of molar yields of C_1-C_5 gases in the pyrolysis of the Springfield coal as a function of thermal maturity (Easy $\%R_o$) (C_4 and C_5 include i-C_4 and n-C_4, i-C_5 and n-C_5, respectively). The comparison of gas yields in this study with the kinetic calculations are shown (Tang et al., 1996; Zhang et al., 2008; Tian et al., 2008; Li et al., 2021; Li and Horita, in revision).

Fig. 2. Total hydrocarbon gas yields (C_1-C_5) and molar ratios ($C_1/(C_1$-$C_5)$) with maturities, compared with kinetic model on gas generation from immature Barnett Shale (Hill et al., 2007) and gas ratios on the pyrolysis of Cameo coal (Zhang et al., 2008).

Fig. 3. Carbon and hydrogen isotopic compositions of CH_4, C_2H_6 and C_3H_8 in the pyrolysis gases from Springfield coal.

Fig. 4. Position-specific carbon isotope deviations of propane ($\Delta C_{c\text{-}t} = \delta^{13}C_{center} - \delta^{13}C_{terminal}$) in the pyrolysis of Springfield coal, with the comparison of results from the pyrolysis of Woodford Shale (Li and Horita, in revision) and the cracking of n-C_{25} (Gilbert et al., 2019) and C_3H_8 (Li et al., 2021), as well as the equilibrium model (Webb and Miller, 2014).

Fig. 5. Position-specific $\delta^{13}C$ values of propane in hydrous and anhydrous pyrolysis conditions as a function of maturity (Easy $\%R_o$).

Fig. 6. Bulk carbon isotope fractionation of C_1-C_3 in the pyrolysis of Springfield coal (this study), marine Woodford Shale (Li and Horita, in revision) in the temperature range of 310 to 480 ^oC. The theoretical calculations on the KIE in the cracking of n-alkane (Tang et al., 2000) and n-C_8 (Ni et al., 2011), and experimental study of C_3H_8 cracking (Li et al., 2021) are presented, with C KIE of CH_4 in the low-temperature pyrolysis of different kerogens (Wei et al., 2018) and of C_1-C_3 at high-temperature pyrolysis of xylite (Berner et al., 1995).

Fig. 7. Position-specific carbon isotope fractionation of propane from the cracking of the Springfield coal (this study), Woodford Shale (Li and Horita, in revision), n-alkane (Tang et al., 2000), n-C_8 (Ni et al., 2011) and C_3H_8 (Li et al., 2021) in the temperature range from 310 to 480 ^oC.

Fig. 8. Summary of $\delta^{13}C_{ter}$ and $\delta^{13}C_{cen}$ values of propane from this study, natural and pyrolysis gases (Suda et al., 2017; Liu et al., 2018, 2019; Piasecki et al., 2018; Gilbert et al., 2019; Zhao et al., 2020; Zhang et al., 2022; Li and Horita, in revision), compared with theoretical modeling on n-C_{40} and n-C_{20} cracking (Peterson et al., 2018), C_3H_8 cracking (Li et al., 2021), biodegradation (Gilbert et al., 2019), and diffusion (Piasecki et al., 2016).

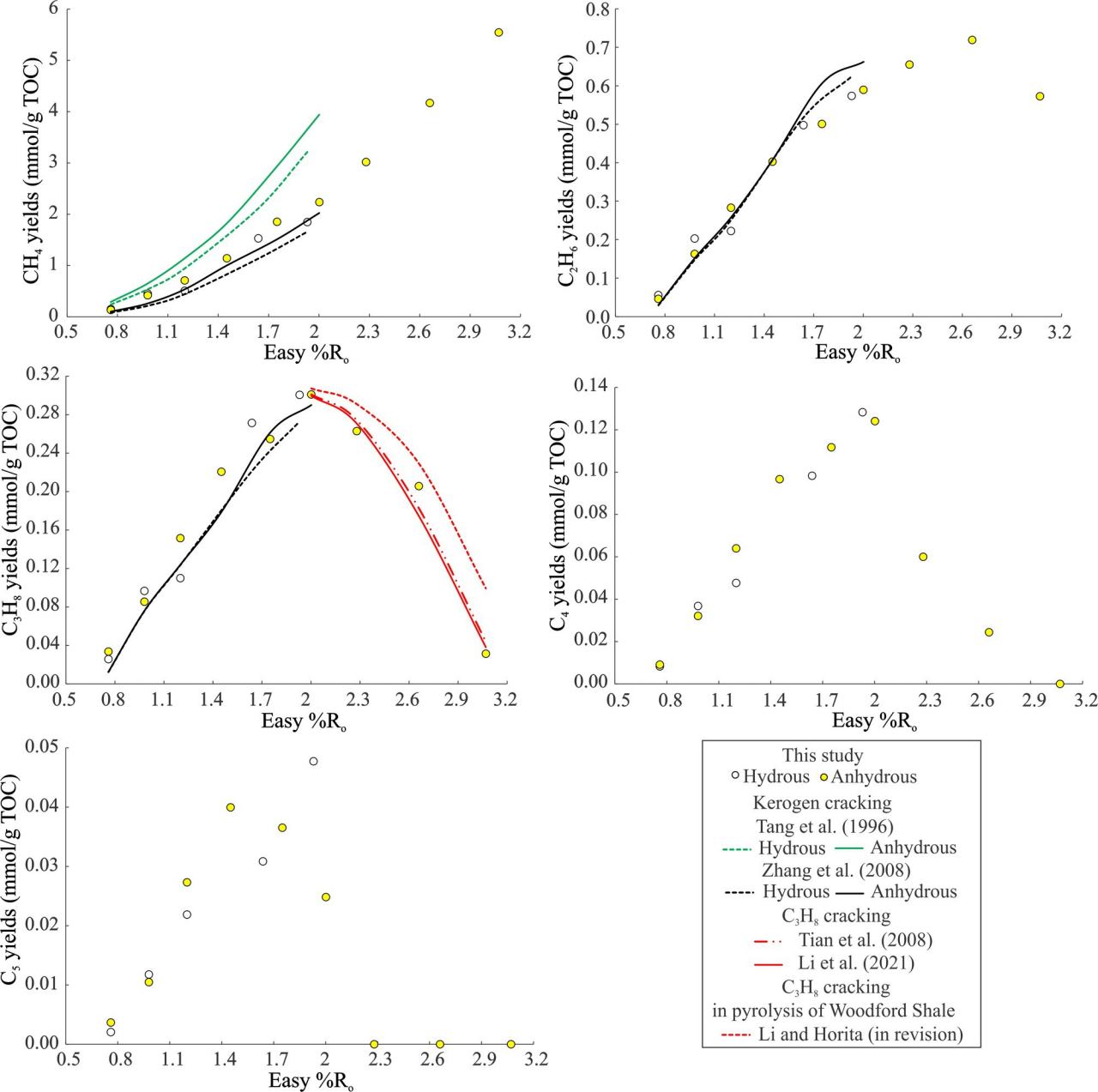
CH4 yields (mmol/g TOC)
Easy %Ro
C2H6 yields (mmol/g TOC)
Easy %Ro
C3H8 yields (mmol/g TOC)
Easy %Ro
C4 yields (mmol/g TOC)
Easy %Ro
C5 yields (mmol/g TOC)
Easy %Ro
This study
Hydrous Anhydrous
Kerogen cracking
Tang et al. (1996)
Hydrous Anhydrous
Zhang et al. (2008)
Hydrous Anhydrous
C3H8 cracking
Tian et al. (2008)
Li et al. (2021)
C3H8 cracking
in pyrolysis of Woodford Shale
Li and Horita (in revision)

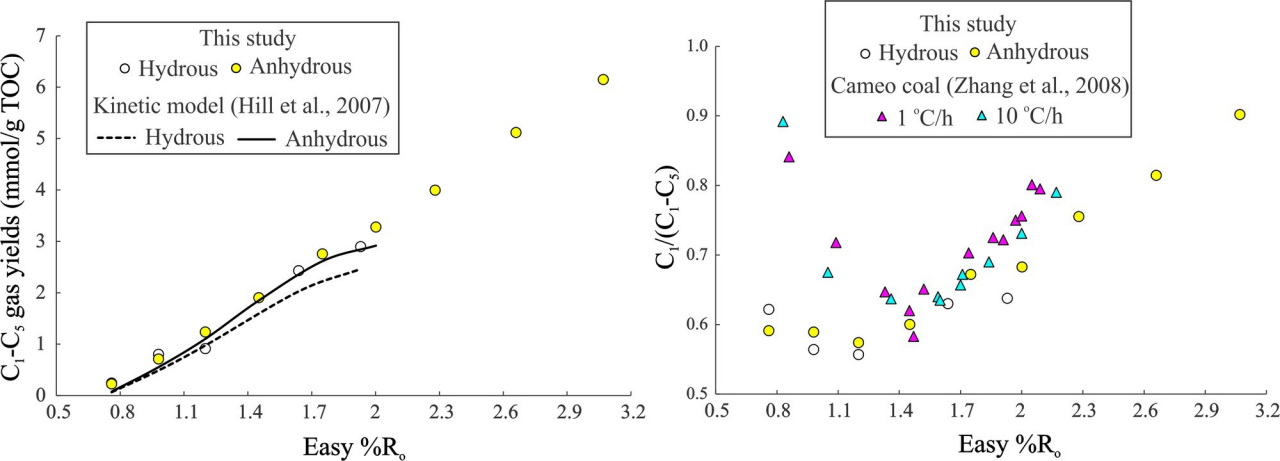
This study
Hydrous
Anhydrous
Kinetic model (Hill et al., 2007)
Hydrous
Anhydrous
C1-C5 gas yields (mmol/g TOC)
Easy %Ro
This study
Hydrous
Anhydrous
Cameo coal (Zhang et al., 2008)
1 °C/h
10 °C/h
C1/(C1-C5)
Easy %Ro

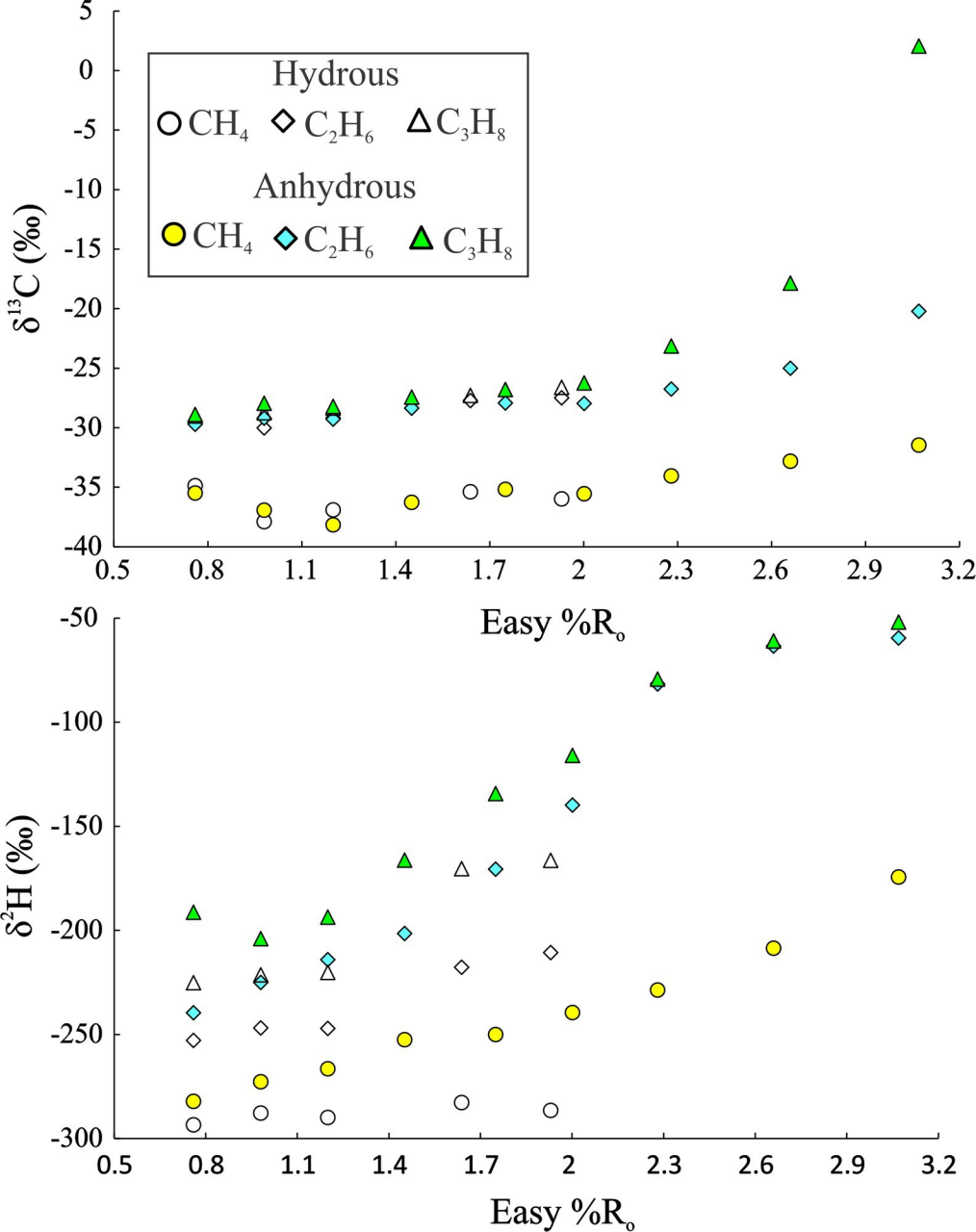
Hydrous
CH4 C2H6 C3H8
Anhydrous
CH4 C2H6 C3H8
δ13C (‰)
5
0
-5
-10
-15
-20
-25
-30
-35
-40
0.5
0.8
1.1
1.4
1.7
2
2.3
2.6
2.9
3.2
Easy %Ro
δ2H (‰)
-50
-100
-150
-200
-250
-300
0.5
0.8
1.1
1.4
1.7
2
2.3
2.6
2.9
3.2
Easy %Ro

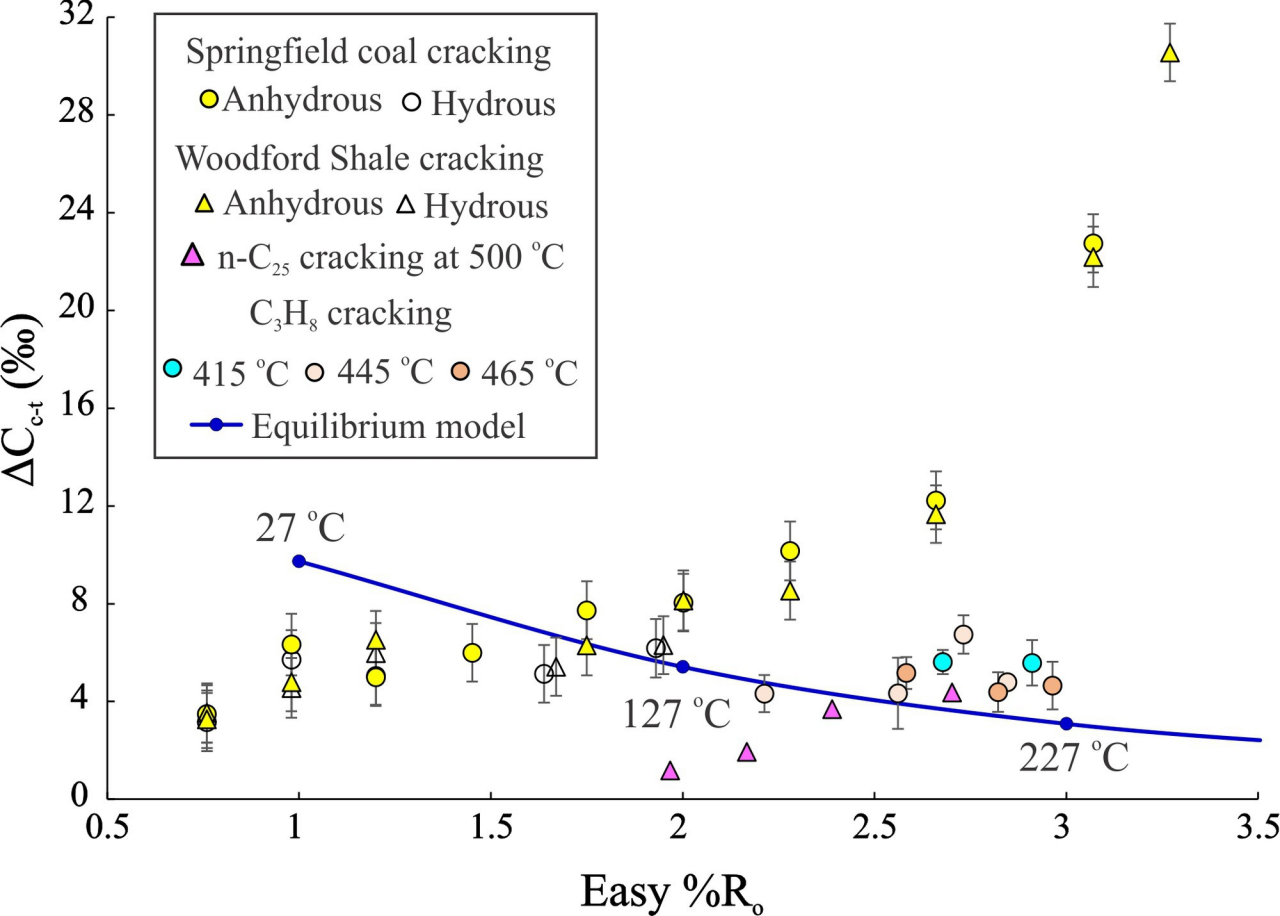
Springfield coal cracking
Anhydrous
Hydrous
Woodford Shale cracking
Anhydrous
Hydrous
n-C25 cracking at 500 °C
C3H8 cracking
415 °C
445 °C
465 °C
Equilibrium model
27 °C
127 °C
227 °C
ΔCc-t (‰)
Easy %Ro
0
4
8
12
16
20
24
28
32
0.5
1
1.5
2
2.5
3
3.5

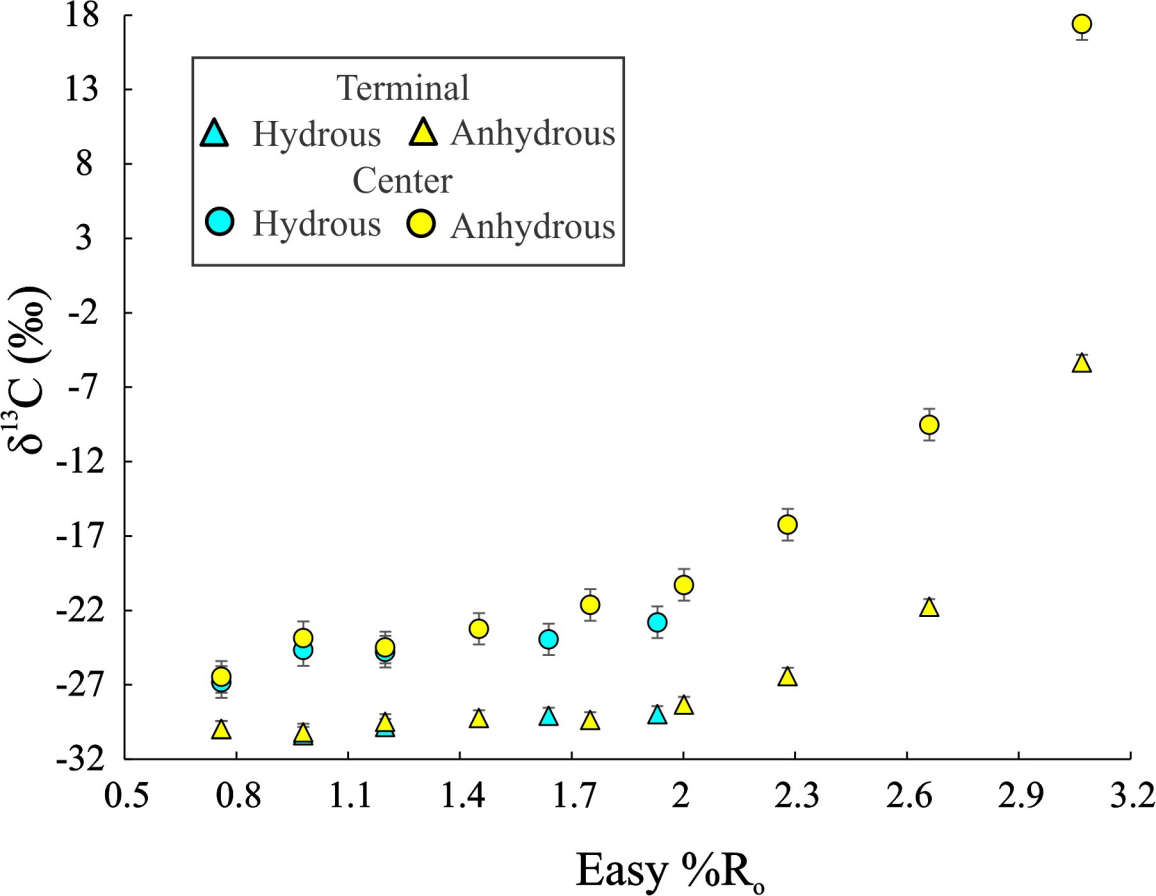
Terminal
Hydrous
Anhydrous
Center
Hydrous
Anhydrous
δ13C (‰)
18
13
8
3
-2
-7
-12
-17
-22
-27
-32
0.5
0.8
1.1
1.4
1.7
2
2.3
2.6
2.9
3.2
Easy %Ro

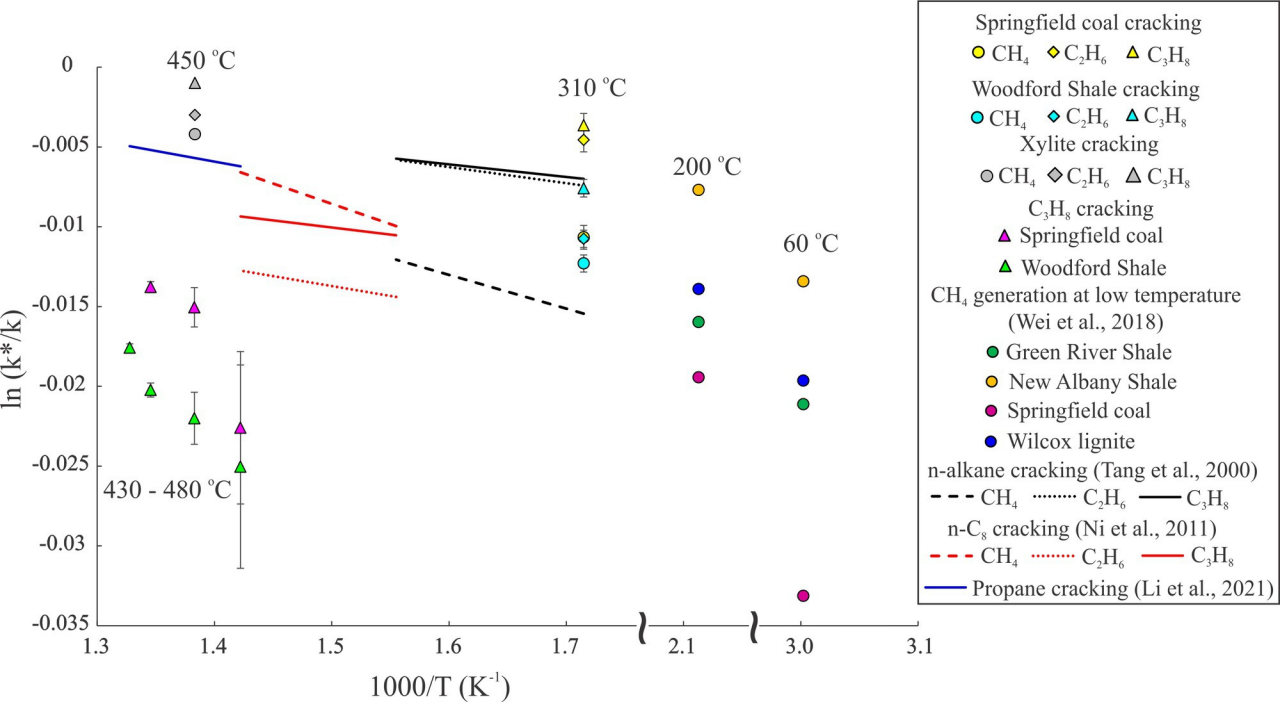
0
-0.005
-0.01
-0.015
-0.02
-0.025
-0.03
-0.035
ln (k*/k)
1.3
1.4
1.5
1.6
1.7
2.1
3.0
3.1
1000/T (K-1)
450 °C
310 °C
200 °C
60 °C
430 - 480 °C
Springfield coal cracking
CH4 C2H6 C3H8
Woodford Shale cracking
CH4 C2H6 C3H8
Xylite cracking
CH4 C2H6 C3H8
C3H8 cracking
Springfield coal
Woodford Shale
CH4 generation at low temperature (Wei et al., 2018)
Green River Shale
New Albany Shale
Springfield coal
Wilcox lignite
n-alkane cracking (Tang et al., 2000)
CH4 C2H6 C3H8
n-C8 cracking (Ni et al., 2011)
CH4 C2H6 C3H8
Propane cracking (Li et al., 2021)

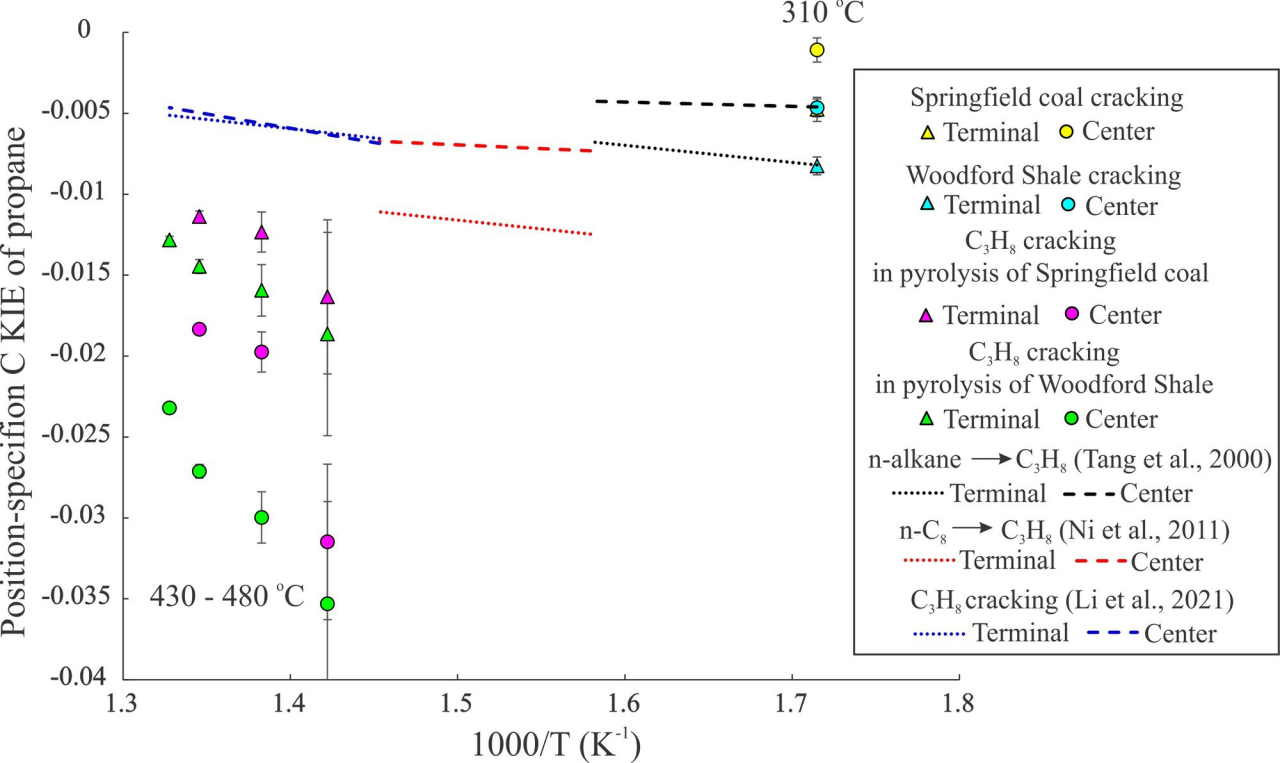
310 °C
430 - 480 °C
Position-specifion C KIE of propane
1000/T (K-1)
0
-0.005
-0.01
-0.015
-0.02
-0.025
-0.03
-0.035
-0.04
1.3
1.4
1.5
1.6
1.7
1.8
Springfield coal cracking
Terminal
Center
Woodford Shale cracking
Terminal
Center
C3H8 cracking
in pyrolysis of Springfield coal
Terminal
Center
C3H8 cracking
in pyrolysis of Woodford Shale
Terminal
Center
n-alkane → C3H8 (Tang et al., 2000)
Terminal
Center
n-C8 → C3H8 (Ni et al., 2011)
Terminal
Center
C3H8 cracking (Li et al., 2021)
Terminal
Center

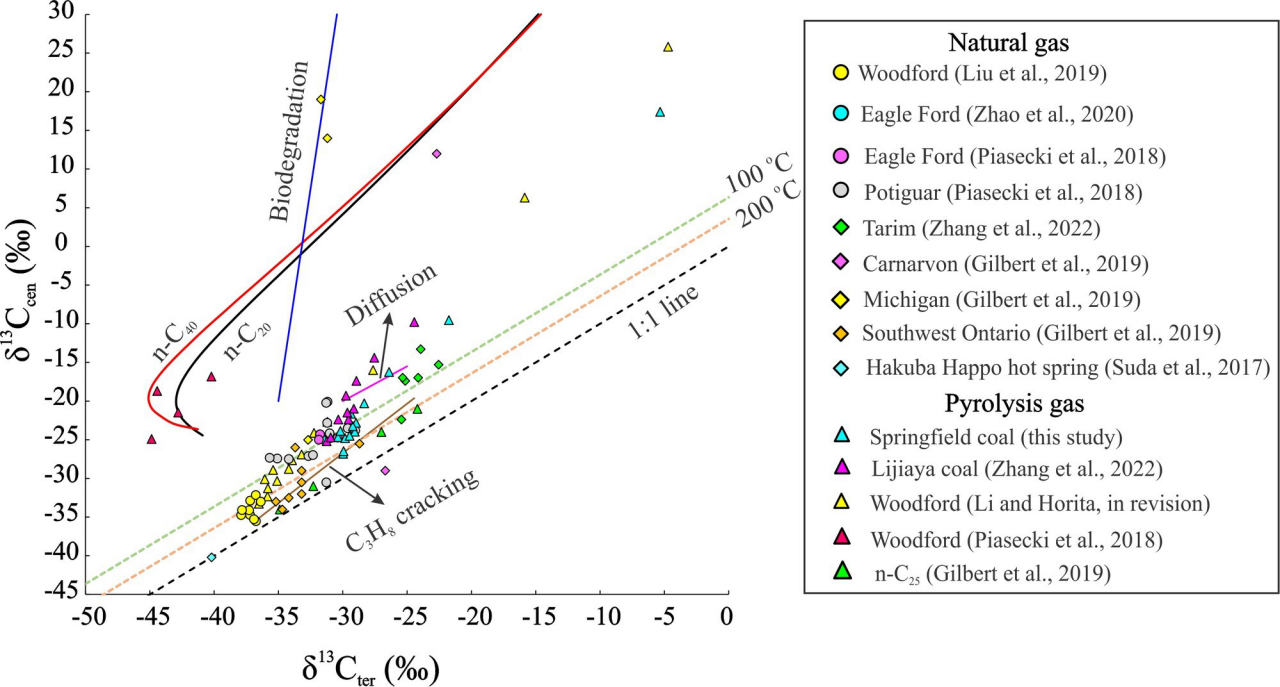
Natural gas
Woodford (Liu et al., 2019)
Eagle Ford (Zhao et al., 2020)
Eagle Ford (Piasecki et al., 2018)
Potiguar (Piasecki et al., 2018)
Tarim (Zhang et al., 2022)
Carnarvon (Gilbert et al., 2019)
Michigan (Gilbert et al., 2019)
Southwest Ontario (Gilbert et al., 2019)
Hakuba Happo hot spring (Suda et al., 2017)
Pyrolysis gas
Springfield coal (this study)
Lijiaya coal (Zhang et al., 2022)
Woodford (Li and Horita, in revision)
Woodford (Piasecki et al., 2018)
n-C25 (Gilbert et al., 2019)
Biodegradation
Diffusion
n-C40
n-C20
100 °C
200 °C
1:1 line
C3H8 cracking
δ13Ccen (‰)
δ13Cter (‰)
30
25
20
15
10
5
0
-5
-10
-15
-20
-25
-30
-35
-40
-45
-50
-45
-40
-35
-30
-25
-20
-15
-10
-5
0

Table 1. Experimental conditions and measured yields of gaseous species produced from the isothermal closed-system pyrolysis of Springfield coal in the temperature range of 310 to 470 ºC.

Table 2. Isotope compositions of the HC gases from the pyrolysis of Springfield coal in different experimental conditions.

Table 3. Position-specific C isotopes of propane generated in the hydrous and anhydrous pyrolysis of Springfield coal. ($\delta^{13}C_{ter}$: $\delta^{13}C$ in terminal position of propane; $\delta^{13}C_{cen}$: $\delta^{13}C$ at central position of propane; ΔC_{c-t}: position-specific carbon isotope deviation ($\delta^{13}C_{cen}$ - $\delta^{13}C_{ter}$); std: standard deviation)

Type	T (°C)	Easy %R_o	HC gas yield (C_1-C_5) (mmol/g TOC)	Gas yield (mmol/g TOC)								$C_1/(C_1-C_5)$
				CH_4	C_2H_6	C_3H_8	C_4	C_5	H_2	CO_2	H_2S	
Hy	310	0.76	0.24	0.15	0.06	0.03	0.01	0.00	0.01	0.53	0.00	0.62
	340	0.98	0.76	0.43	0.19	0.09	0.03	0.01	0.10	0.86	0.16	0.56
	360	1.2	0.91	0.51	0.22	0.11	0.05	0.02	0.13	0.90	0.44	0.56
	370	1.67	2.43	1.53	0.50	0.27	0.10	0.03	0.09	1.28	0.33	0.63
	370	1.95	2.90	1.85	0.57	0.30	0.13	0.05	0.12	1.30	0.94	0.64
Anhy	310	0.76	0.23	0.13	0.05	0.03	0.01	0.00	0.01	0.30	0.00	0.59
	340	0.98	0.71	0.42	0.16	0.09	0.03	0.01	0.06	0.43	0.02	0.59
	360	1.2	1.24	0.71	0.28	0.15	0.06	0.03	0.11	0.40	0.13	0.57
	380	1.45	1.90	1.14	0.40	0.22	0.10	0.04	0.09	0.44	0.13	0.60
	400	1.75	2.76	1.85	0.50	0.25	0.11	0.04	0.09	0.59	0.10	0.67
	415	2.00	3.28	2.24	0.59	0.30	0.12	0.02	0.12	0.51	0.15	0.68
	430	2.28	4.00	3.02	0.66	0.26	0.06	0.00	0.15	0.58	0.35	0.76
	450	2.66	5.12	4.17	0.72	0.21	0.02	0.00	0.21	0.59	0.24	0.81
	470	3.07	6.15	5.55	0.57	0.03	0.00	0.00	0.32	0.57	0.00	0.90

Easy %R_o is calculated based on temperature and time program in the pyrolysis experiments according to Sweeney and Burnham (1990).

Hy: hydrous experiments; Anhy: anhydrous experiments.

CO_2 and H_2S yields in hydrous conditions include measured gaseous amounts and calculated yields in the solution.

Type	T (°C)	Easy %R_o	$\delta^{13}C$ (‰)								$\delta^{2}H$ (‰)								
			CH_4	C_2H_6	C_3H_8	i-C_4	n-C_4	i-C_5	n-C_5	CO_2	CH_4	C_2H_6	C_3H_8	i-C_4	n-C_4	i-C_5	n-C_5	H_2	H_2S
Hy	310	0.76	-34.9	-29.5	-29.0	-28.9	-28.3	-27.3	-29.0	-20.5	-293	-253	-225	-192	-201	-174	-204	-423	
	340	0.98	-37.9	-30.0	-28.7	-29.2	-27.9	-27.8	-27.6	-21.2	-288	-247	-221	-178	-199	-168	-198	-393	-536
	360	1.2	-36.9	-29.2	-28.4	-29.7	-27.6	-27.8	-27.1	-23.2	-290	-247	-220	-179	-197	-164	-189	-388	-535
	370	1.64	-35.4	-27.7	-27.3	-28.2	-26.8	-27.1	-26.9	-22.6	-283	-218	-170	-151	-148	-129	-158	-372	-539
	370	1.93	-36.0	-27.5	-26.6	-27.7	-26.5	-26.6	-26.5	-23.0	-287	-211	-166	-147	-145	-123	-149	-387	-536
Anhy	310	0.76	-35.5	-29.7	-28.9	-29.2	-28.4	-27.8	-27.9	-22.2	-282	-240	-191	-177	-188	-164	-189	-487	
	340	0.98	-36.9	-29.2	-28.0	-28.5	-27.4	-27.5	-27.5	-22.7	-273	-225	-204	-168	-182	-153	-185	-471	
	360	1.2	-38.2	-29.3	-28.2	-28.4	-27.9	-27.9	-27.7	-22.6	-266	-214	-194	-152	-175	-142	-171	-399	-533
	380	1.45	-36.3	-28.4	-27.4	-28.5	-27.1	-26.8	-26.6	-22.1	-252	-202	-166	-141	-147	-123	-152	-383	-537
	400	1.75	-35.2	-27.9	-26.8	-26.9	-26.0	-22.5	-23.3	-22.8	-250	-171	-134	-126	-119	-92	-119	-408	
	415	2.00	-35.5	-28.0	-26.2	-26.5	-22.2	-15.1	-13.2	-22.5	-239	-140	-116	-94	-88	-54	-89	-320	-535
	430	2.28	-34.0	-26.8	-23.1	-21.2	-9.8			-22.8	-229	-82	-79					-321	-535
	450	2.66	-32.8	-25.0	-17.8	-15.3	-1.3			-22.7	-209	-63	-61					-303	-536
	470	3.07	-31.5	-20.2	2.1					-22.8	-174	-60	-52					-297	-532

Type	T (°C)	Easy %R_o	Position-specific ^{13}C isotope of C_3H_8 (‰)					
			$\delta^{13}C_{ter}$	std	$\delta^{13}C_{cen}$	std	ΔC_{c-t}	std
Hy	310	0.76	-30.0	0.5	-26.8	1.1	3.2	1.2
	340	0.98	-30.4	0.5	-24.7	1.1	5.7	1.2
	360	1.2	-29.8	0.5	-24.8	1.1	5.0	1.2
	370	1.64	-29.1	0.5	-23.9	1.1	5.1	1.2
	370	1.93	-29.0	0.5	-22.8	1.1	6.2	1.2
Anhy	310	0.76	-30.0	0.5	-26.5	1.1	3.5	1.2
	340	0.98	-30.2	0.6	-23.9	1.1	6.3	1.3
	360	1.2	-29.5	0.5	-24.5	1.1	5.0	1.2
	380	1.45	-29.2	0.5	-23.2	1.1	6.0	1.2
	400	1.75	-29.4	0.5	-21.6	1.1	7.7	1.2
	415	2.00	-28.3	0.5	-20.3	1.1	8.0	1.2
	430	2.28	-26.4	0.6	-16.2	1.1	10.2	1.2
	450	2.66	-21.8	0.5	-9.5	1.1	12.2	1.2
	470	3.07	-5.3	0.5	17.4	1.1	22.7	1.2